Journal of Power Sources 189 (2009) 145–148

Contents lists available at ScienceDirect

Journal of Power Sources

journal homepage: www.elsevier.com/locate/jpowsour

Short communication

High-rate performance of all-solid-state lithium secondary batteries using $Li_4Ti_5O_{12}$ electrode

Hirokazu Kitaura, Akitoshi Hayashi*, Kiyoharu Tadanaga, Masahiro Tatsumisago

Department of Applied Chemistry, Graduate School of Engineering, Osaka Prefecture University, 1-1 Gakuen-cho, Naka-ku, Sakai, Osaka 599-8531, Japan

ARTICLE INFO

Article history:
Received 27 June 2008
Accepted 5 October 2008
Available online 11 October 2008

Keywords:
All-solid-state cells
Lithium secondary batteries
$Li_4Ti_5O_{12}$
Negative electrode
Solid electrolyte
High-rate performance

ABSTRACT

The all-solid-state Li–In/$Li_4Ti_5O_{12}$ cell using the $80Li_2S{\cdot}20P_2S_5$ (mol%) solid electrolyte was assembled to investigate rate performances. It was difficult to obtain the stable performance at the charge current density of 3.8 mA cm^{-2} in the all-solid-state cell. In order to improve the rate performance, the pulverized $Li_4Ti_5O_{12}$ particles were applied to the all-solid-state cell, which retained the reversible capacity of about 90 mAh g^{-1} at 3.8 mA cm^{-2}. The $70Li_2S{\cdot}27P_2S_5{\cdot}3P_2O_5$ glass–ceramic, which exhibits the higher lithium ion conductivity than the $80Li_2S{\cdot}20P_2S_5$ solid electrolyte, was also used. The Li–In/$70Li_2S{\cdot}27P_2S_5{\cdot}3P_2O_5$ glass–ceramic/pulverized $Li_4Ti_5O_{12}$ cell was charged at a current density higher than 3.8 mA cm^{-2} and showed the reversible capacity of about 30 mAh g^{-1} even at 10 mA cm^{-2} at room temperature.

1. Introduction

Rechargeable batteries for eco-cars such as EV and HEV have been studied from the viewpoint of environment conservation. Lithium ion batteries with high power and high energy density are strong candidates for the electric vehicle batteries. However, applying the conventional lithium batteries to large-scale batteries is difficult because of their safety hazards. The fabrication of all-solid-state lithium batteries with inorganic solid electrolytes can resolve such safety issues [1,2]. We have developed Li_2S–P_2S_5 solid electrolytes [3] and applied the $80Li_2S{\cdot}20P_2S_5$ (mol%) glass–ceramic with high lithium ion conductivity of about 10^{-3} S cm^{-1} to all-solid-state cells [4,5]. In addition, we recently discovered that the $70Li_2S{\cdot}(30-x)P_2S_5{\cdot}xP_2O_5$ glass–ceramics showed the extremely high conductivities of over 10^{-3} S cm^{-1} [6,7].

Various electrode active materials were applied to the all-solid-state batteries using the $80Li_2S{\cdot}20P_2S_5$ glass–ceramic and the batteries worked at low current densities less than 0.1 mA cm^{-2}. However, their high-rate performances have not been investigated extensively and, to our knowledge, few studies about rate performance have been carried out in the bulk-type all-solid-state batteries except for the all-solid-state cells using $LiCoO_2$, carbon, FeS_2, $Cu_2Mo_6S_8$ and α-Fe_2O_3 [8–13]. However, high-rate performances of the solid-state cells are still inferior to those of lithium ion batteries with liquid electrolytes. In order to improve the rate performances of all-solid-state cells, we have focused on composite electrodes, which were composed of an active material, a solid electrolyte and a conductive additive. We reported that the morphologies of the electrode materials significantly influence the cell capacity and the rate performance [9,13,14]. The electrode–electrolyte interface is also important. For example, in the In/$80Li_2S{\cdot}20P_2S_5$ glass–ceramic/$LiCoO_2$ cells, high resistance interface between the $LiCoO_2$ electrode and the solid electrolyte was observed by the AC impedance measurements [15]. The formation of the favorable solid-solid interface between electrodes and electrolytes is indispensable for enhancing electrochemical performance of the all-solid-state batteries.

$Li_4Ti_5O_{12}$ is a promising negative electrode material for all-solid-state batteries because of the several advantages such as good cycle performance and no volume change during the charge–discharge process [16]. We reported that the all-solid-state Li–In/$80Li_2S{\cdot}20P_2S_5$ glass–ceramic/$Li_4Ti_5O_{12}$ cells worked reversibly during more than 300 cycles under a low current density of about 0.064 mA cm^{-2} [17]. In addition, the impedance analysis was performed and it was found that the interfacial resistance in the all-solid-state cell using $Li_4Ti_5O_{12}$ was lower than that of the all-solid-state cell using $LiCoO_2$ [18]. However, the large overvoltage was observed during discharging (lithium insertion process) at the current density of 1.3 mA cm^{-2}. As a result of the impedance analysis, it was found that the resistances of the lithium ion transfer at the electrode–electrolyte interface during a discharge process

* Corresponding author. Tel.: +81 72 2549334; fax: +81 72 2549334.
E-mail address: hayashi@chem.osakafu-u.ac.jp (A. Hayashi).

0378-7753/$ – see front matter © 2008 Elsevier B.V. All rights reserved.
doi:10.1016/j.jpowsour.2008.10.005

are still high in the all-solid-state cells. Therefore, the discharge current density had to be restricted to 0.064 mA cm^{-2}; the all-solid-state cell showed the average charge voltage of 1.9 V (vs. Li) and the reversible capacity of about 80 mAh g^{-1} at 1.3 mA cm^{-2}. It is necessary to evaluate the cell performance at the higher current densities and improve the rate performance.

Shortening the lithium diffusion path is effective for the improvement of rate performances in the lithium ion batteries [19]. The reduction of the cell resistance by the utilization of a solid electrolyte with higher lithium ion conductivity is also required to improve the rate performance. In this study, the rate performance of all-solid-state Li–In/80Li_2S·20P_2S_5 solid electrolyte/$Li_4Ti_5O_{12}$ cells were investigated at current densities higher than 1 mA cm^{-2}. Then the improvement of rate performance was examined. Lithium titanate particles were pulverized to shorten the lithium diffusion path. In addition, the 80Li_2S·20P_2S_5 solid electrolyte was replaced with the 70Li_2S·27P_2S_5·3P_2O_5 oxysulfide electrolyte with higher lithium ion conductivity.

2. Experimental

Lithium titanate ($Li_4Ti_5O_{12}$, Titankogyo Co.) was used as an active material and it was confirmed by XRD that the particles were the pure spinel phase. The lithium titanate particles were pulverized by using a planetary ball mill apparatus. The particles were put into a 45-ml alumina pot together with zirconia balls (Ø = 4 mm, 100 balls). Mechanical grinding was carried out at a rotating speed of 200 rpm for 2 h.

All-solid-state electrochemical cells were assembled as follows. The 80Li_2S·20P_2S_5 (mol%) and 70Li_2S·27P_2S_5·3P_2O_5 glasses were prepared by the mechanochemical reaction process [6,9]. The glass–ceramic electrolyte was prepared by crystallizing the glass. The obtained glass–ceramic was used as a solid electrolyte for all-solid-state cells. A composite electrode as a working electrode was prepared by mixing of $Li_4Ti_5O_{12}$ (27.3 wt.%), the solid electrolyte (63.6 wt.%), and acetylene black (9.1 wt.%) powders. The composite electrode (10 mg) and solid electrolyte powder (80 mg) were set in a polycarbonate tube and then were pressed under 360 MPa. Li–In alloy, which was formed by attaching an indium foil (thickness: 300 μm) and lithium foil (thickness: 250 μm), as a counter and reference electrode was put on the solid electrolyte layer and the three-layered pellet was sandwiched by two stainless-steel disks as current collectors. Two electrode cells were obtained after pressing under 120 MPa.

Galvanostatic tests of the cells were conducted at 25 °C in an Ar atmosphere using a charge–discharge measuring device (BTS-2004, Nagano Co.). Electrochemical impedance spectroscopic measurements were performed by applying a small perturbation voltage of 50 mV in the frequency range of 1 MHz to 10 mHz using an impedance analyzer (Solartron 1287 coupled with Solartron 1260). The electrochemical cells discharged or charged to the different depths were analyzed using impedance measurements after the rest for several hours. These measurements were carried out for the cells at the dc potential equal to open circuit voltage (OCV).

3. Results and discussion

Fig. 1 shows the 10th and 20th charge curves and cycling performance of the all-solid-state Li–In/80Li_2S·20P_2S_5 glass–ceramic/$Li_4Ti_5O_{12}$ cells. The cells were discharged at a constant current density of 0.064 mA cm^{-2} during 20 cycles and charged at 1.3 mA cm^{-2} during the initial 10 cycles and at 3.8 mA cm^{-2} during the subsequent 10 cycles. The solid line and solid circles denote the rate performance of the cell using bare $Li_4Ti_5O_{12}$ particles. The cell retained the charge capacity of about 80 mAh g^{-1} at 1.3 mA cm^{-2} during 10 cycles. However, voltage profiles at 3.8 mA cm^{-2} were unstable. In order to improve the rate performance, the lithium titanate particles were pulverized to decrease the particle size. Fig. 2 shows the SEM images of lithium titanate particles before and after pulverization. The spherical particles were observed and their particle size was 1–10 μm in diameter before pulverization. The particle size decreased to less than 1 μm after pulverization; the pulverized particles showed the XRD pattern of spinel phase. Such particles were applied to the all-solid-state cells. The dashed line and open circles in Fig. 1 denote the rate performance of the cell using pulverized $Li_4Ti_5O_{12}$ particles. The cell using pulverized particles showed the stable behavior in the charge curve at 3.8 mA cm^{-2} and retained the charge capacity of 90 mAh g^{-1} during 20 cycles. The improvement of the high-rate performance is due to shortening the lithium diffusion path because no differences of the impedance spectra was observed between the cells using bare particles and pulverized particles. However, the cell using pulverized particles showed the unstable voltage profiles at much higher current density of 6.4 mA cm^{-2}.

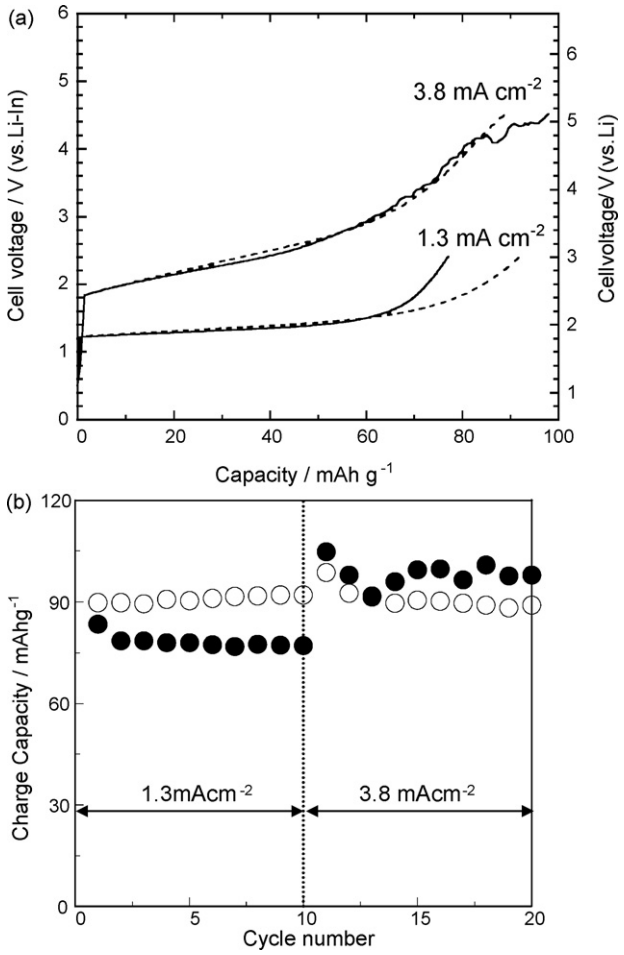

Fig. 1. The 10th and 20th charge curves (a), and cycling performance (b), of the all-solid-state Li–In/80Li_2S·20P_2S_5 glass–ceramic/$Li_4Ti_5O_{12}$ (solid line and solid circles) and pulverized $Li_4Ti_5O_{12}$ (dashed line and open circles) cells. The cells were discharged at a constant current density of 0.064 mA cm^{-2} and charged at 1.3 mA cm^{-2} in the initial 10 cycles and at 3.8 mA cm^{-2} in the subsequent 10 cycles.

In order to improve the electrochemical performance of all-solid-state cells, we applied the 70Li_2S·27P_2S_5·3P_2O_5 glass–ceramic as a solid electrolyte to the cell using pulver-

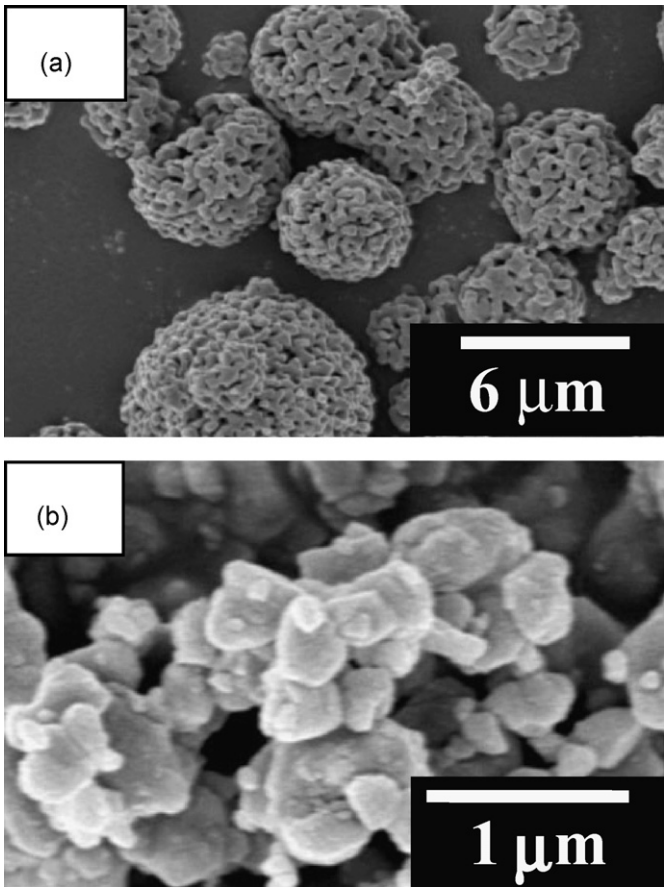

Fig. 2. SEM images of $Li_4Ti_5O_{12}$ before (a), and after (b), pulverization for 2 h.

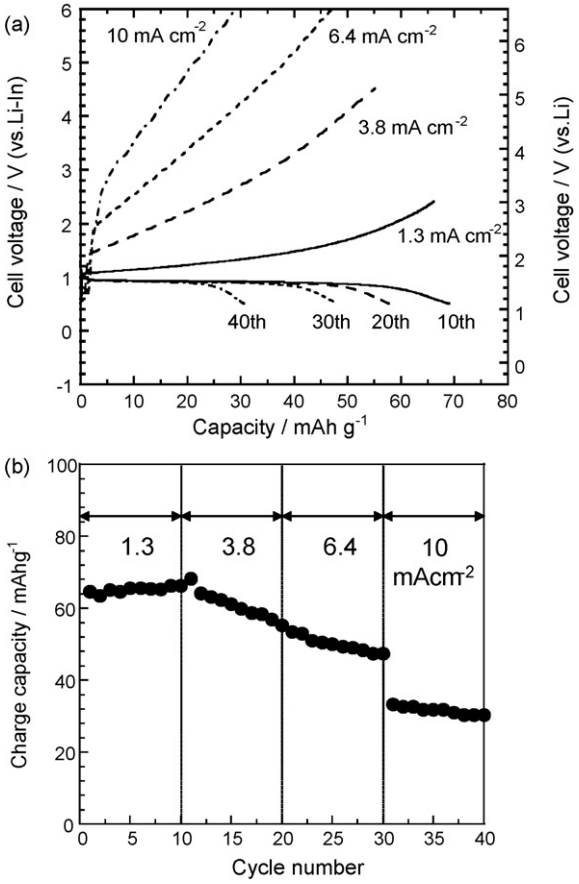

Fig. 3. Charge–discharge curves (a), and cycling performance (b), of the all-solid-state Li–In/$70Li_2S{\cdot}27P_2S_5{\cdot}3P_2O_5$ glass–ceramic/pulverized $Li_4Ti_5O_{12}$ cell. The cells were discharged at a constant current density of 0.064 mA cm^{-2} and charged at the current densities from 1.3 mA cm^{-2} to 10 mA cm^{-2} during 50 cycles.

ized $Li_4Ti_5O_{12}$ particles. Fig. 3 shows the charge–discharge curves and cycling performance of the Li–In/$70Li_2S{\cdot}27P_2S_5{\cdot}3P_2O_5$ glass–ceramic/pulverized $Li_4Ti_5O_{12}$ cell. The charge–discharge measurements were conducted by changing the charge current density from 1.3 to 10 mA cm^{-2}. The discharge current density was kept constant at 0.064 mA cm^{-2} during 40 cycles. The all-solid-state cell worked as a rechargeable lithium battery. The stable voltage profiles were obtained at the current density from 1.3 to 10 mA cm^{-2}. The cell maintained the charge capacity of 66 mAh g^{-1} at 1.3 mA cm^{-2} during 10 cycles. However, the capacity gradually decreased during subsequent 20 cycles at 3.8 and 6.4 mA cm^{-2}. The cell then showed a drastic decline of the capacity in the 31st cycle and retained the charge capacity of about 30 mAh g^{-1} at 10 mA cm^{-2}. The large overvoltage was observed and the charge curves became tilted. Although the reason has not been clarified, the large overvoltage may be related to the lithium diffusion within the lithium titanate.

Fig. 4 shows the impedance spectra of the Li–In/$80Li_2S{\cdot}20P_2S_5$ glass–ceramic/$Li_4Ti_5O_{12}$ cell (a) and Li–In/$70Li_2S{\cdot}27P_2S_5{\cdot}3P_2O_5$ glass–ceramic/pulverized $Li_4Ti_5O_{12}$ cell (b) after discharging to 1.1 V (vs. Li) at 0.064 mA cm^{-2}. The total resistance decreased by replacing the $80Li_2S{\cdot}20P_2S_5$ glass–ceramic with the $70Li_2S{\cdot}27P_2S_5{\cdot}3P_2O_5$ glass–ceramic. The three resistive components were observed in the high (>1 MHz), middle (250 kHz) and low (1 Hz) frequency regions on the cell (a). On the other hand, two resistive components were observed in the high (>25 kHz) and low (1 Hz) frequency regions on the cell (b). From our previous study [18], the resistance in the high frequency region is ascribed to the resistance of the solid electrolyte layer between a working

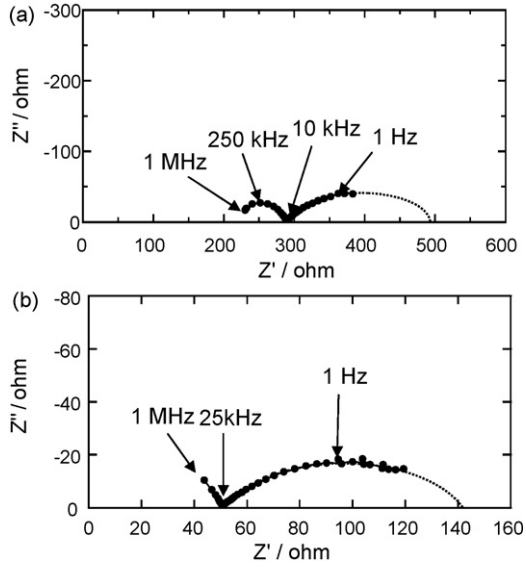

Fig. 4. Nyquist plots of Li–In/$80Li_2S{\cdot}20P_2S_5$ glass–ceramic/$Li_4Ti_5O_{12}$ cell (a), and Li–In/$70Li_2S{\cdot}27P_2S_5{\cdot}3P_2O_5$ glass–ceramic/pulverized $Li_4Ti_5O_{12}$ cell (b), after discharging to 1.1 V (vs. Li).

electrode and a counter electrode in Fig. 4(a). The resistance in the middle frequency region was derived from the composite electrode. In Fig. 4(b), the resistance in the high frequency region, which may contain the resistance derived from the composite electrode, is mainly attributable to the resistance of the solid electrolyte layer. The value of 50 Ω is almost the same as the resistance measured by sandwiching the $70Li_2S{\cdot}27P_2S_5{\cdot}3P_2O_5$ glass–ceramic with stainless-steel plates as ion-blocking electrodes. The resistance of the solid electrolyte on the cell (b) was the smaller than that on the cell (a). The rate performance was improved due to the reduction of the resistance of the solid electrolyte.

The resistance in the low frequency region (1 Hz) can be ascribed to the resistance of the lithium ion transfer at the electrode–electrolyte interface in Fig. 4(a) because the resistance was not observed before charge–discharge measurements and was observed only during discharging [18]. Such a behavior agrees with the behavior of the resistance in the low frequency region (1 Hz) on the cell (b). The resistance in the low frequency region is therefore interpreted as the resistance of the lithium ion transfer at the interface between the lithium titanate and the $70Li_2S{\cdot}27P_2S_5{\cdot}3P_2O_5$ solid electrolyte. The resistance of the lithium ion transfer at the electrode–electrolyte interface decreased by using $70Li_2S{\cdot}27P_2S_5{\cdot}3P_2O_5$ glass–ceramic. The decrease of the resistance of the lithium ion transfer would improve the rate performance during discharge measurements.

4. Conclusions

The Li–In/$Li_4Ti_5O_{12}$ cells using Li_2S–P_2S_5 solid electrolyte were assembled and the rate performances were investigated. The application of the smaller $Li_4Ti_5O_{12}$ particles and the solid electrolyte with the higher lithium ion conductivity was effective for the improvement of the rate performance. The all-solid-state cell using $70Li_2S{\cdot}27P_2S_5{\cdot}3P_2O_5$ solid electrolyte showed the reversible capacity of about 30 mAh g^{-1} even at the high charge current density of 10 mA cm^{-2} after discharging at 0.064 mA cm^{-2}.

Acknowledgments

This work was supported by a Grant-in-Aid for Scientific Research from the Ministry of Education, Culture, Sports, Science and Technology of Japan, and also supported by the New Energy and Industrial Technology Development Organization (NEDO) of Japan.

References

[1] C. Julien, G.-A. Nazri, Solid State Batteries: Materials Design and Optimization, Kluwer Academic Publishers, Boston, 1994, p. 579.
[2] J.-M. Tarascon, M. Armand, Nature 414 (2001) 359.
[3] F. Mizuno, A. Hayashi, K. Tadanaga, M. Tatsumisago, Solid State Ionics 177 (2006) 2721.
[4] A. Hayashi, S. Hama, H. Morimoto, M. Tatsumisago, T. Minami, Chem. Lett. (2001) 872.
[5] M. Tatsumisago, F. Mizuno, A. Hayashi, J. Power Sources 159 (2006) 193.
[6] F. Mizuno, A. Hayashi, K. Tadanaga, M. Tatsumisago, Adv. Mater. 17 (2005) 918.
[7] K. Minami, A. Hayashi, M. Tatsumisago, Solid State Ionics, in press.
[8] K. Iwamoto, N. Aotani, K. Takada, S. Kondo, Solid State Ionics 79 (1995) 288.
[9] F. Mizuno, A. Hayashi, K. Tadanaga, M. Tatsumisago, Solid State Ionics 177 (2006) 2731.
[10] K. Takada, T. Inada, A. Kajiyama, H. Sasaki, S. Kondo, M. Watanabe, M. Murayama, R. Kanno, Solid State Ionics 158 (2003) 269.
[11] B.C. Kim, K. Takada, N. Ohta, Y. Seino, L. Zhang, H. Wada, T. Sasaki, Solid State Ionics 176 (2005) 2383.
[12] R. Kanno, M. Murayama, T. Inada, T. Kobayashi, K. Sakamoto, N. Sonoyama, A. Yamada, S. Kondo, Electrochem. Solid-State Lett. 7 (2004) A455.
[13] H. Kitaura, K. Takahashi, F. Mizuno, A. Hayashi, K. Tadanaga, M. Tatsumisago, J. Electrochem. Soc. 154 (2007) A725.
[14] F. Mizuno, A. Hayashi, K. Tadanaga, M. Tatsumisago, J. Electrochem. Soc. 152 (2005) A1499.
[15] A. Sakuda, H. Kitaura, A. Hayashi, K. Tadanaga, M. Tatsumisago, Electrochem. Solid-State Lett. 11 (2008) A1.
[16] T. Ohzuku, A. Ueda, N. Yamamoto, J. Electrochem. Soc. 142 (1995) 1431.
[17] M. Tatsumisago, A. Hayashi, J. Non-Cryst. Solids 354 (2008) 1411.
[18] H. Kitaura, A. Hayashi, K. Tadanaga, M. Tatsumisago, J. Electrochem. Soc. (2008), in press.
[19] C. Jiang, M. Ichihara, I. Honma, H. Zhou, Electrochim. Acta 52 (2007) 6470.